SPE-170685-MS

Effect of Confinement on PVT Properties of Hydrocarbons in Shale Reservoirs

T. Pitakbunkate, and P. B. Balbuena, Texas A&M University; G. J. Moridis, Lawrence Berkeley National Laboratory; T. A. Blasingame, Texas A&M University

This paper was prepared for presentation at the SPE Annual Technical Conference and Exhibition held in Amsterdam, The Netherlands, 27–29 October 2014.

Abstract

Shale reservoirs play an important role as a future energy resource of the United States. Numerous studies have been performed to describe the storage and transport of hydrocarbons through ultra-small pores in the shale reservoirs. Most of these studies were developed by modifying techniques used for conventional reservoirs. The common pore size distribution of the shale reservoirs is approximately 1-20 nm and in such confined spaces the interactions between the wall of the container (i.e., the shale and kerogen) and the contained fluids (i.e., the hydrocarbon fluids and water) may exert significant influence on the localized phase behavior. We believe this is due to the fact that the orientation and distribution of fluid molecules in the confined space are different from those of the bulk fluid; causing changes in the localized thermodynamic properties.

This study provides a detailed account of the changes of PVT properties and phase behavior (specifically, the phase diagrams) in a synthetic shale reservoir for pure hydrocarbons (methane and ethane) and a simple methane-ethane (binary) mixture. Grand Canonical Monte Carlo (GCMC) simulations are performed to study the effect of confinement on the fluid properties. A graphite slab made of two layers is used to represent kerogen in the shale reservoirs. The separation between the two layers, representing a kerogen pore, is varied from 1 nm to 10 nm to observe the changes of the hydrocarbon fluid properties. In this paper, the critical properties of methane and ethane as well as the methane-ethane mixture phase diagrams in different pore sizes are derived from the GCMC simulations. In addition, the GCMC simulations are used to investigate the deviations of the fluid densities in the confined space from those of the bulk fluids at reservoirs conditions. While not investigated in this work, such deviations may indicate that significant errors for production forecasting and reserve estimation in shale reservoirs may occur if the (typical) bulk densities are used in reservoir engineering calculations.

Introduction

Over the past decade, the main focus of the petroleum industry has to develop the technology exploit shale reservoirs. Unlike conventional sandstone and carbonate reservoirs, shale reservoirs have unique rock properties — in particular, ultra-low in-situ permeabilities (on the order of 1-100 nd is very common). Shale reservoirs contain nano-scale sized pores, which leads to the ultra-low permeabilities, but also some

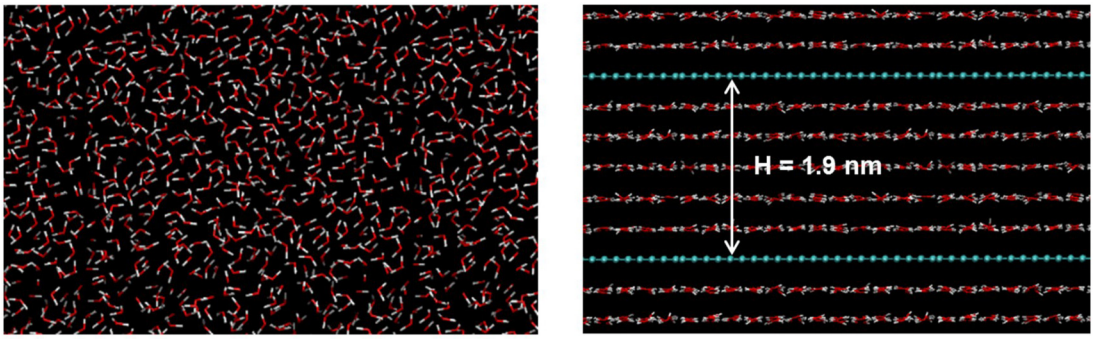

Figure 1—(a) Snapshot of bulk water molecules and (b) Snapshot of water molecules confined between graphite slabs.

very unusual phase behavior caused by "confinement" in very small pores. Consequently, it is nearly impossible to extract hydrocarbon fluids from shale reservoirs without substantial "stimulation" of the formation, and the current favored model is that of the multi-fractured horizontal well. The ultra-low permeability nature of these reservoirs, combined with the requirement of significant reservoir stimulation to achieve commercial flowrates has led to the descriptor of "unconventional reservoirs" for shale gas and liquids-rich shale reservoirs.

As noted, numerous studies have been performed to describe the storage and transport of hydrocarbons in shale reservoirs; in particular to improve reserves estimation and production forecasts. Desorption-adsorption models (e.g., the Langmuir model) are added in numerical reservoir simulation and gas-in-place calculation to account for adsorbed gas in shales (Shabro et al. 2011; Ambrose et al. 2011; Ambrose et al. 2012; Das et al.). In ultra-small pores, turbulent flow may develop and cause deviation from the conventional models (i.e., Darcy's equation). Knudsen's number is used to characterize slip and no-slip flow and Knudsen diffusion and slip flow models are incorporated to improve the accuracy of the numerical simulation (Freeman 2010; Shabro et al. 2011; Darabi et al. 2012, Fathi et al. 2012). However, most of these studies were developed by modifying techniques used for conventional reservoirs — only a few of these studies consider the fundamental effects of pore size on hydrocarbon PVT properties and flow behavior (i.e., storage and transport of fluids).

The common pore size distribution of the shale reservoirs is approximately 1-20 nm. (Nagarajan et al. 2013). In such a confined space, interaction between the wall of the container (i.e., shale and kerogen) and the contained fluid (i.e., hydrocarbons) becomes significant to the fluid's behavior. As a result, equations of state derived for bulk fluid (i.e., Peng-Robinson, Redlich-Kwong) may not be valid for PVT calculation in the shale reservoirs. **Figure 1** illustrates the difference of molecular orientation and arrangement of bulk water and that of confined water from Molecular Dynamics (MD) simulations at room temperature and a density of 0.86 g/cm^3. Molecules in bulk water move randomly without specific orientation and direction. On the other hand, water molecules in the slit graphite pore with 1.9 nm of separation between the two layers (measured from the center of a graphite layer to the center of the other one) have a well-ordered, layered structure in the horizontal direction arranged in planes parallel to the graphite surfaces. Such structural differences can cause the change of fluid phase behavior and thermodynamic properties. It is reported that the water mobility of confined water becomes significantly lower than that of bulk water (Hirunsit and Balbuena 2006). In addition, Zarragoicoechea et al. 2004 have shown that the shifts on the critical temperature are proportional to the size of the mesopore. Normally, as the pore size decreases, the critical temperature and freezing/melting point tend to decrease (Kenda et al. 2004; Moore et al. 2010).

In this work, we focus on establishing phase transitions and critical points of pure components of methane and ethane and phase diagrams of a methane-ethane mixture in confined spaces emulating those

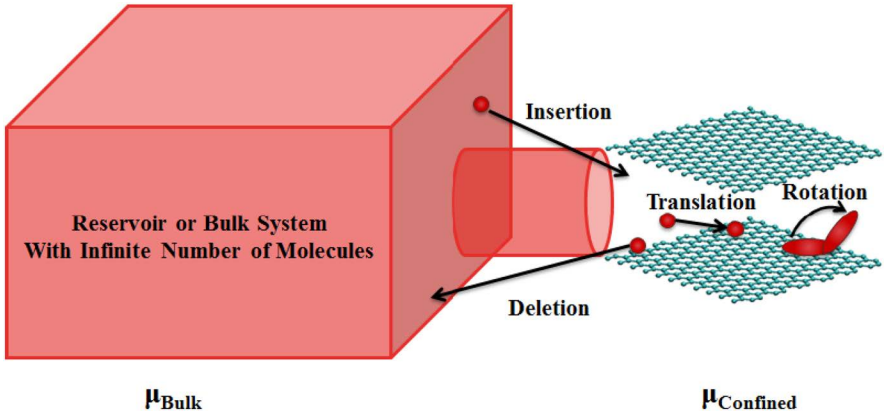

Figure 2—Schematic of GCMC simulation.

in shale reservoirs. More specifically, we model kerogen in the shale reservoirs as slit pores with graphene walls representing different pore sizes. Moreover, the deviations of confined fluid densities from the bulk of each component at the reservoir conditions are shown to emphasize that significant error may be involved when using bulk properties for reserves estimation or production forecast calculations.

Molecular Simulation Procedures

Grand Canonical Monte-Carlo (GCMC) simulations

In thermodynamics, the chemical potential (μ) is the free energy per mole which physically represents the escaping tendency for a molecular component immersed in a system. For instance, a system with high chemical potential has a high tendency for fluid particles to escape and flow to a system of lower chemical potential. In statistical mechanics, a grand canonical ensemble is a statistical ensemble that is used to represent the possible states of a system that is being maintained in thermodynamic equilibrium with a reservoir or with a bulk system at given conditions of chemical potential μ, temperature T and volume V. This ensemble is sometimes called the μVT ensemble. In Grand Canonical Monte Carlo simulations (GCMC), μ, T, and V, are constant while the number of molecules (n) fluctuates. The chemical potential of the bulk system (reservoir) is calculated from the given temperature and pressure using classical equations of state. To represent equilibrium, the reservoir is connected to the ensemble (our confined system) as shown in **Figure 2**, and various types of motion are allowed by the GCMC simulation to emulate the evolution of the system to the equilibrium state Thus, during simulation, the GCMC algorithm randomly chooses to act on the confined system from the following choices for a molecule in the confined fluid volume:

a. a molecule is created at a random position (insertion);
b. a molecule is displaced (translation);
c. a molecule is removed (deletion);
d. a molecule is rotated (rotation, for non-spherical molecules)

At each step one of the four events takes place, and the system energy is computed. The simulation proceeds until reaching thermodynamic equilibrium where the chemical potential of the bulk and the confined system are equal:

$$\mu_{Bulk}(T,p) = \mu_{Confined} \quad (1)$$

Force Fields

The chemical potential of the confined system is computed from a given force field. In this study, the Optimized Potential for Liquid Simulations (OPLS) model (Jorgensen et al. 1984) is used for methane and

Table 1—L-J potential parameters for CH_4 - CH_4, CH_3 - CH_3 (in ethane) and C - C (in graphite) interactions.

Pair interaction	σ_{ii}, Å	ϵ_{ii}/k, K
CH_4 - CH_4	3.730	148.0
CH_3 - CH_3	3.775	104.1
C - C	3.400	28.0

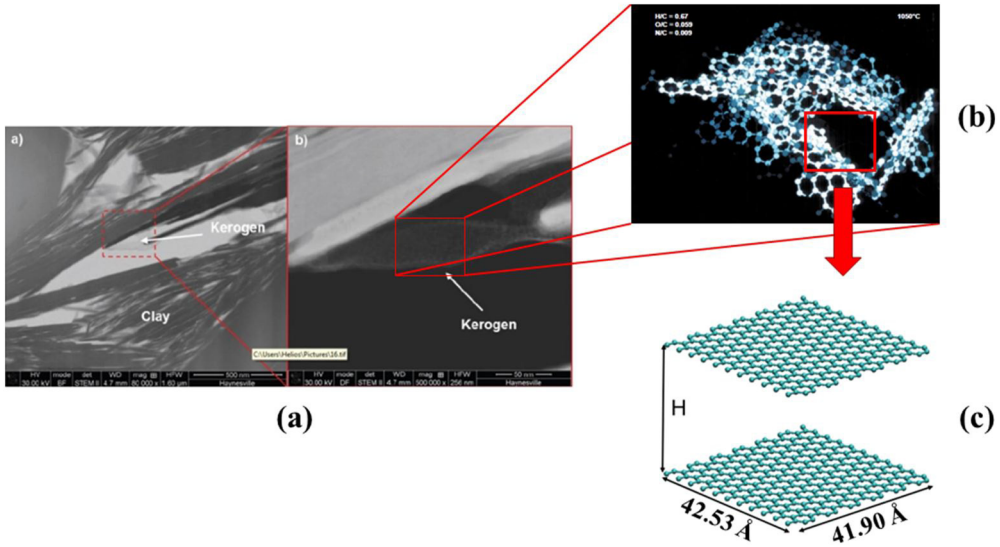

Figure 3—(a) STM image of Haynesville shale (Curtis et al. 2010), (b) 3D molecular structure of kerogen (Vandenbroucke 2003) and (c) molecular model representing kerogen in shale reservoirs.

ethane. The Lennard-Jones potential parameters of carbon atoms in graphite are from Kurniawen et al. (2006). The methane molecule is represented as a single sphere and the ethane molecule is represented by two spheres of methyl groups connected by a single bond of 1.54 Å. Van der Waals interactions between molecules are described by a 12-6 Lennard-Jones potential.

$$U(r_{ij}) = \begin{cases} 4\epsilon_{ij}\left[\left(\frac{\sigma_{ij}}{r_{ij}}\right)^{12} - \left(\frac{\sigma_{ij}}{r_{ij}}\right)^{6}\right] & ; r_{ij} \le r_c \\ 0 & ; r_{ij} > r_c \end{cases} \quad (2)$$

ϵ_{ij} and σ_{ij} are the LJ potential parameters that characterize the molecular size and strength of the intermolecular interactions and r_{ij} is the distance between the centers of mass of the molecular pair. r_c is the cut-off distance beyond which the interaction between i and j molecules is assumed negligible. In this work, the minimum half-cell distance of the system is used as the r_c value. However, r_c should be equal or greater than $5 \times \max(\sigma_{ij})$ where the potential or interaction between the molecules becomes insignificant. The model parameters of the like interaction are given in **Table 1**, whereas those for the unlike interaction are determined by the Lorentz-Berthelot combining rules:

$$\sigma_{ij} = \frac{\sigma_{ii}+\sigma_{jj}}{2} \quad (3a)$$

$$\epsilon_{ij} = \sqrt{\epsilon_{ii}\epsilon_{jj}} \quad (3b)$$

Building the Model System

Figure 3a illustrates an example of the Scanning Tunneling Microscopy (STM) image of Haynesville shale (Curtis et al. 2010). Shale reservoirs consist of inorganic (i.e., clay) and organic matter known as

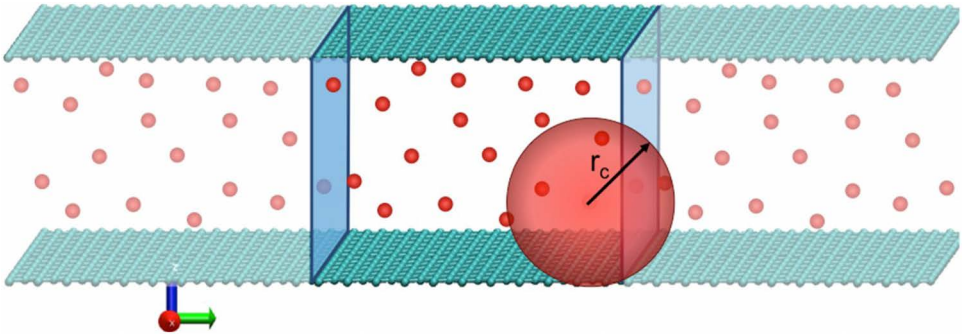

Figure 4—Periodic boundary conditions used to extend the simulated system to represent kerogen pore network.

kerogen. Hydrocarbon is stored in the shale reservoirs in both pores in the rock and kerogen pores. **Figure 3b** illustrates an example of 3D molecular structure of kerogen (Vandenbroucke 2003). It can be observed that the kerogen pore can be modeled in first approximation by a slit graphite pore. Here the slit pore model is constructed so that graphite-like crystallites are semi-infinite and composed of the two-layer graphite slabs aligned parallel to one another and separated by a distance, *H*, as shown in **Figure 3c**. The value of the separation is varied from 1 nm to 10 nm. The dimensions of the graphite slabs are 42.53 Å × 41.90 Å.

Periodic boundary conditions are applied to extend the simulated system to a pore network and account for interactions between molecules at the edge of the system and molecules in the next periodic cell (identical to the simulated system) as shown in **Figure 4**.

Analysis of the Simulation Data

The GCMC simulation allows us to evaluate the equilibrium density of the confined fluid at given conditions of temperature and pressure. This density can be computed for each of the components in a mixture thus yielding adsorption isotherms as functions of gas pressure. The adsorption is computed as the amount of molecules present in the unit cell (system) at equilibrium conditions, i.e., where the chemical potentials (of all phases for each component) of both the reservoir (bulk fluid) and the confined system are equal at given conditions of temperature and pressure.

$$\mu^{vapor}_{Bulk,CH_4}(T,p) = \mu^{vapor}_{Confined,CH_4} = \mu^{liquid}_{Confined,CH_4} \tag{4a}$$

And

$$\mu^{vapor}_{Bulk,C_2H_6}(T,p) = \mu^{vapor}_{Confined,C_2H_6} = \mu^{liquid}_{Confined,C_2H_6} \tag{4b}$$

Because of the effect of the interaction between fluid molecules and the surface wall, the fluid density in the bulk and the confined space may be different. Once the number of molecules per unit cell (n) are obtained from the GCMC simulations, the density can be computed using the following formula:

$$\rho_{Confined} = \frac{n \times M}{N_A \times V_{Unit\ Cell}} \tag{5}$$

where M is the molecular weight of the fluid, n is the number of molecules per unit cell, N_A is Avogadro's number, and $V_{Unit\ Cell}$ is unit cell volume (excluding the volume occupied by the graphite slab). The calculated fluid density in the confined space is used to determine the critical point of a pure component. At $T < T_c$, a phase transition can be observed when there is an occurrence of a jump of fluid density (from vapor to liquid) while pressure increases. On the other hand, at $T \geq T_c$, the fluid density is a continuous function of pressure and this phase is a called supercritical fluid. As a result, a tip of a phase envelope that contains a two-phase region may yield a critical point of a pure component.

To draw a phase diagram and find critical properties of a *hydrocarbon mixture*, phase transitions of the mixture with different compositions must be determined. Again, the isotherm of the confined system

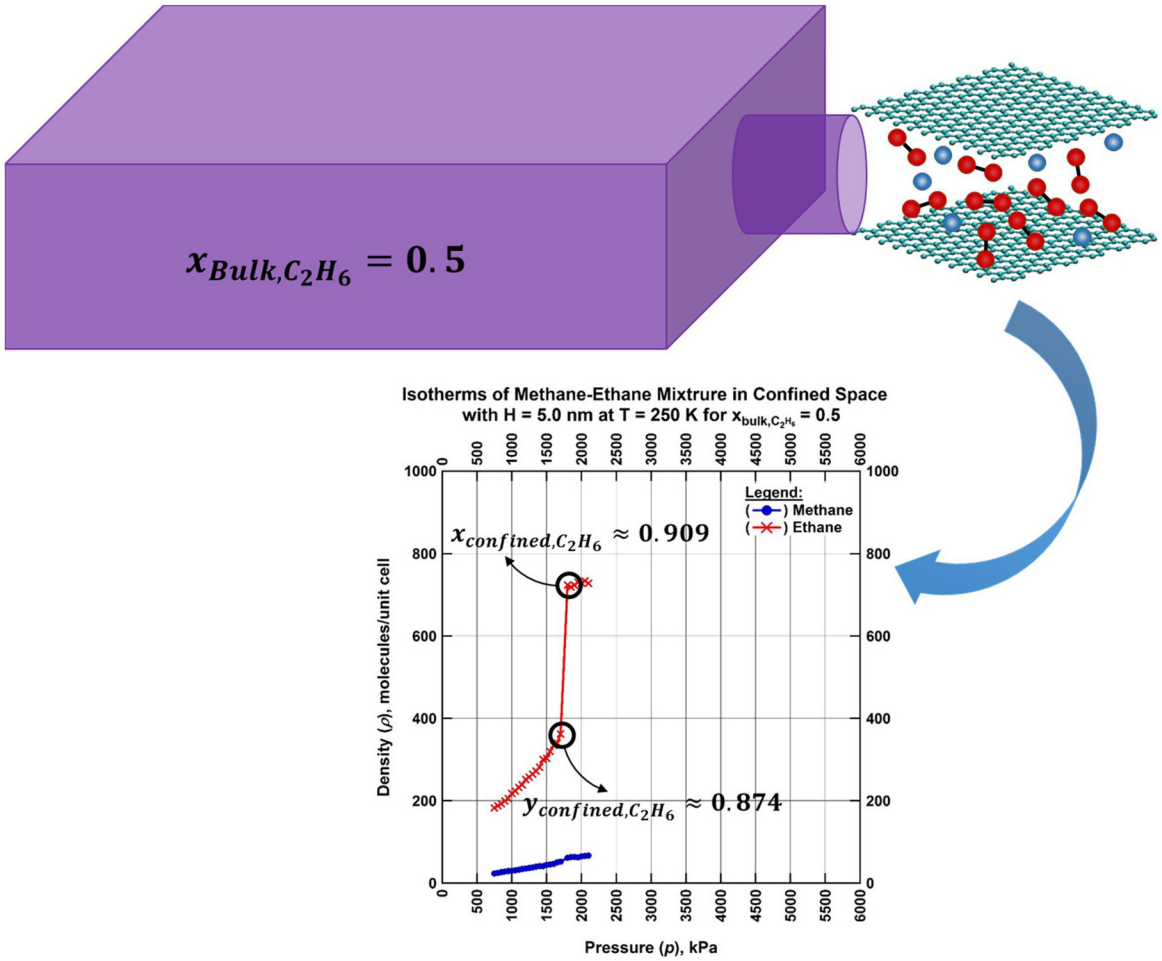

Figure 5—Comparison of fluid composition in the bulk gas phase and that in the confined space distributed in a high density phase (liquid), and in a low density phase (vapor).

obtained from the GCMC simulation must satisfy Eqs. 4a and 4b for each of the components of the mixture. The chemical potential of each component in the confined system is dependent on the interactions of both components among themselves and with the walls of the pore. Thus, the overall fluid composition as specified in the bulk may differ from that in the confined pore as shown in **Figure 5**. Note that **Figure 5** illustrates only a single pore. In the actual system there could be an interconnected pore network, which may have a pore size distribution. Here we study the equilibrium between one specified pore size and the bulk system. In **Figure 5**, the GCMC simulation is set to a temperature of 250K and an ethane molar composition of 50% in the reservoir (x_{Bulk,C_2H6}) to determine isotherms of methane and ethane in the confined system.

According to the isotherms of the confined mixture shown in **Figure 5**, the equilibrium composition of the confined pore is a two-phase mixture having ethane in vapor ($y_{Confined,C_2H6}$) (87.4%) and liquid ($x_{Confined,C_2H6}$) phases (90.9%). These results indicate that the original gas mixture splits into two phases both of them rich in ethane.. Multiple scenarios of this type of simulation with different fluid compositions are needed to generate a phase diagram or P-x diagram (pressure-composition) for a mixture. Once isotherms for each component are acquired, the fluid composition in vapor and liquid phase at the saturation pressure of the mixture can be computed. Consequently, these data are used to create a phase diagram and obtain a critical point of the mixture. **Figure 6a** illustrates isotherms of a methane-ethane mixture indicating phase transition in a slit graphite pore with 5.0 nm of separation for different fluid composition at 250K of temperature. **Figure 6b** is a corresponding P-x diagram. This P-x diagram is at

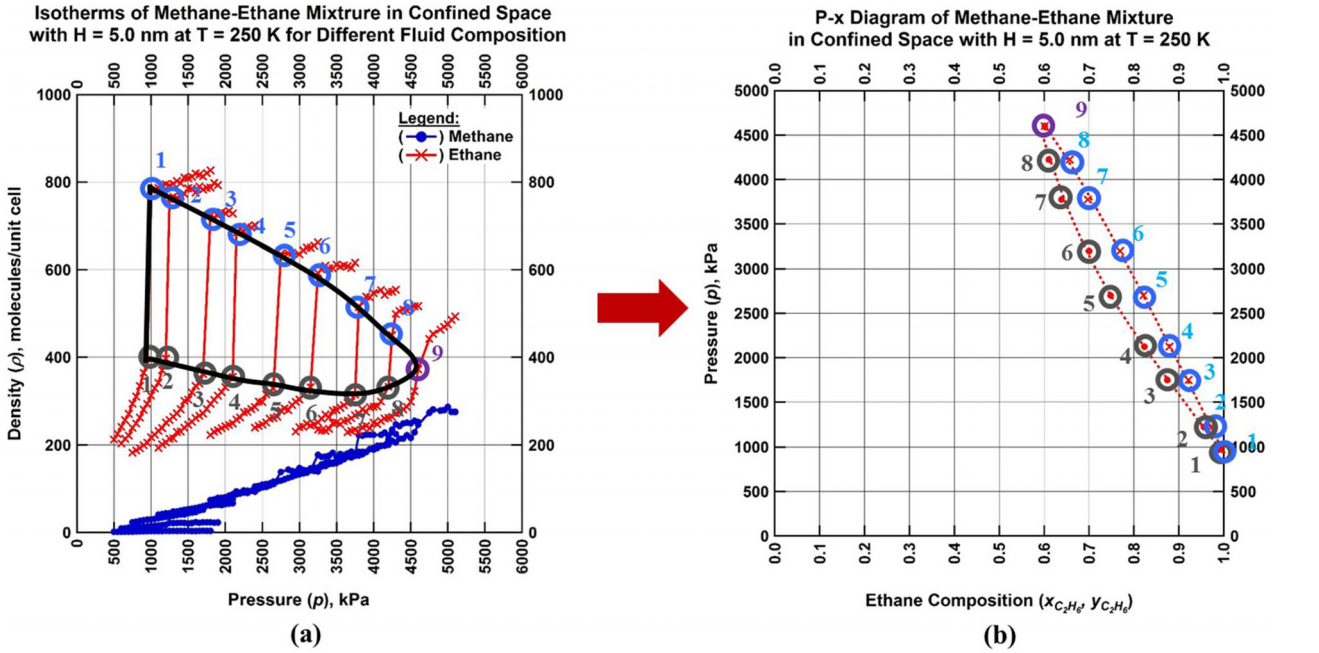

Figure 6—(a) Isotherms of the methane-ethane mixture in a slit graphite pore with 5.0 nm of separation at T = 250 K and (b) the P-x diagram of the mixture corresponding to the isotherms.

constant temperature (T = 250 K). The critical point, shown as the purple line (no. 9), can be seen in **Figures 6a** and **6b**. The line connecting critical points of the mixture with different fluid compositions is called the critical locus curve. This curve can be obtained from drawing a line passing through critical points of P-x diagrams at different temperatures. It is used to approximate critical properties of mixture as a function of fluid composition.

Results and Discussions

The Critical Points of Pure Components in Confined Space

Methane **Figure 7** illustrates an example of a calculated phase diagram for confined methane in a 5.0 nm separation slit graphite pore representing kerogen in shale reservoirs. The GCMC simulations are performed to derive methane isotherms at different temperatures. At higher temperatures, the first-order phase transitions vanish at the critical points as pressure increases and the isotherm becomes a continuous function of pressure at supercritical conditions. On the other hand, at lower temperatures, a jump or discontinuity of the fluid density (from vapor to liquid) occurs while pressure increases. Such a jump is called a first-order phase transition. A phase envelope of the confined methane containing a two-phase region can be drawn by connecting points of vapor and liquid densities at vapor pressures at different temperatures as shown as a black envelope in **Figure 7**. The critical properties can be read from the tip of the envelope. In this case, the critical

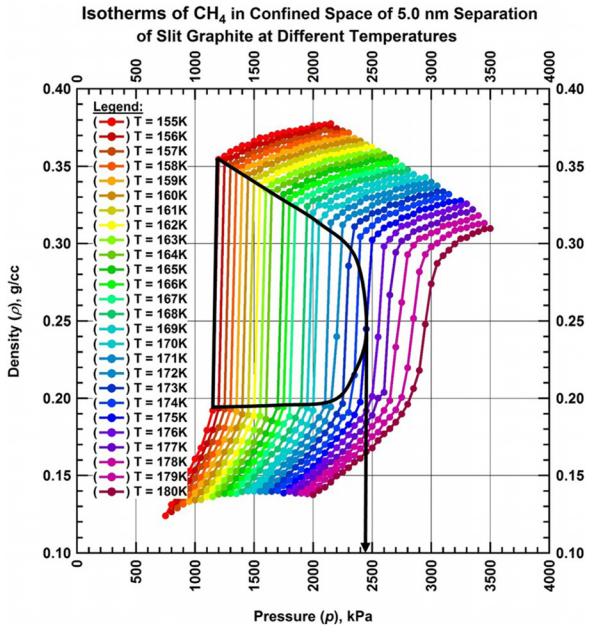

Figure 7—Phase diagram of confined methane in 5.0 nm of separation of a slit graphite pore (representing kerogen in shale reservoir).

Table 2—Critical properties of confined methane in different pore sizes.

Separation (H), nm	Critical temperature (T_c)	Critical pressure (p_c)
1.0	99 K or −281.5°F	4.0×10^{-4} kPa or 5.8×10^{-4} psi
2.0	127 K or −231.1°F	34 kPa or 5 psi
3.0	155 K or −180.7°F	610 kPa or 88 psi
4.0	169 K or −155.5°F	1625 kPa or 236 psi
5.0	175 K or −144.7°F	2450 kPa or 355 psi
6.0	178 K or −139.3°F	2950 kPa or 428 psi
7.0	181.5 K or −133.0°F	3550 kPa or 515 psi
Bulk Fluid	190.45 K or −116.9°F	4600 kPa or 667 psi

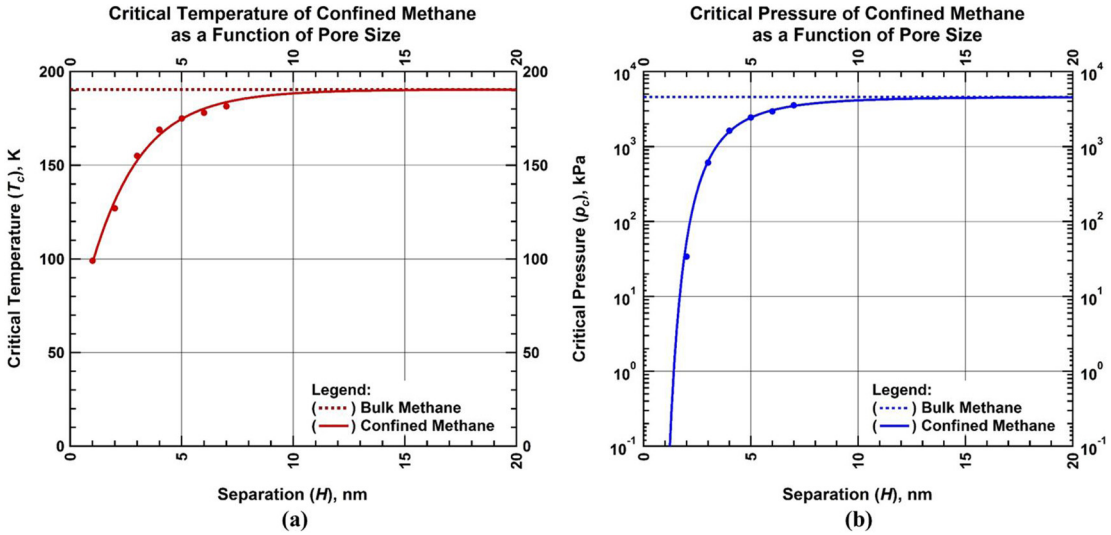

Figure 8—(a) Plot of critical temperature and (b) critical pressure of confined methane versus separation of a slit graphite pore (representing kerogen in shale reservoir).

temperature and pressure of the confined methane in a 5.0 nm separation of slit graphite pore are approximately 175 K or −144.7°F and 2450 kPa or 355 psi, respectively. These procedures are applied to determine the critical properties of confined methane in different pore sizes as summarized in **Table 2**.

Remark: Phase transition was not observed when $H > 7.0$ nm due to a numerical problem

According to the data in **Table 2**, it is noticeable that for the nano-scale pore size, the fluid critical properties change with the pore size and become different from the bulk properties. This is because the interactions between the pore wall and the fluid molecules become significant and impact the behavior of the fluid molecules. The smaller the pore is, the lower both critical temperature and pressure of the confined methane are. At low pressure, with the same temperature, the confined methane is denser than the bulk fluid because the attractive potential of the surface wall allows fluid molecules to adhere to the walls of the confining system and also to interact strongly with each other. Consequently, the confined fluid condenses at lower pressure than the bulk fluid does. This phenomenon may shift the phase envelope to lower critical temperature and pressure, and different critical density.

Figures 8a and **8b** are plots of the critical temperature and pressure of the confined methane versus pore size (separation between the two graphite layers representing the kerogen pore). It can be observed that when $H \leq 5.0$ nm, the critical properties decay rapidly due to the strong effect of the confinement. In addition, as the separation increases, those properties of the confined methane approach the bulk critical properties. Based on this indication, the effect of confinement on the fluid behavior reduces when the pore size increases, as the fluid properties become closer to the bulk properties.

These observations agree with the hypothesis that interaction between the wall of the container and the contained fluid becomes significant to the fluid's behavior and causes the changes of fluid properties. However, this effect is negligible when the pore is adequately large. Consequently, for sufficiently large pores the fluid can be treated as a bulk fluid.

Ethane The same method shown in the previous section is applied to obtain critical points of the confined ethane. **Figure 9** illustrates an example of the phase diagram of confined ethane in a 5.0 nm separation of a slit graphite pore. The phase envelope (black envelope) contains a two-phase region. The critical temperature and pressure of the confined ethane read from the tip of the envelope are approximately 292 K or 66.9°F and 2450 kPa or 355 psi respectively. The critical properties of the confined ethane in different pore sizes are summarized in **Table 3**.

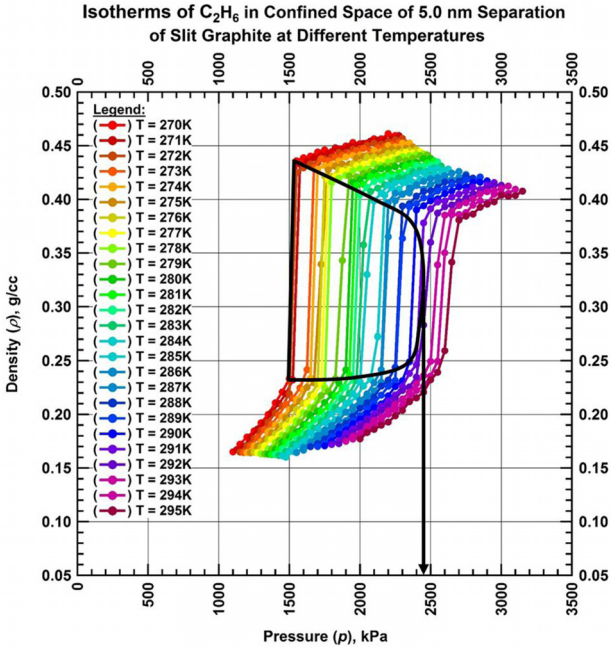

Figure 9—Phase diagram of confined ethane in 5.0 nm of separation of a slit graphite pore (representing kerogen in shale reservoir).

Similar to the case of confined methane, the critical properties of confined ethane are dependent on the pore size. Both the critical temperature and pressure decrease when the pore is smaller. **Figures 10a** and **10b** are plots of those properties versus pore size. It can be observed that when $H \leq 5.0$ nm, the critical properties decay rapidly. This reduction rate of confined ethane is faster than that of confined methane, especially when $H \leq 2.0$ nm because the separation is almost as long as the effective length of the ethane molecule. The effect of the interaction between the surface wall and the confined fluid becomes less significant when the pore size increases and its critical properties approach the bulk properties.

Phase Diagram of a Confined Methane-Ethane Mixture

In the previous section it was shown that the effect of confinement caused the reduction of critical temperature and pressure of pure components of confined methane and ethane in slit graphite pores. For confined methane-ethane mixtures, interactions between the surface wall and the fluid molecules also affect the shape of the mixture phase envelope and critical properties such as a critical locus curve. **Figure 11a** illustrates a bulk phase diagram of a methane-ethane mixture derived from experimental data from Bloomer et al. (1953). The diagram contains a collection of the mixture phase envelopes (P-x diagram) at different temperatures. Connecting the critical points of each envelope yields a critical locus curve as shown by the maroon line in the plot. The area above the curve is a supercritical region. The intersection between the curve and the y-axis at $x_{bulk,C_2}H_6 = 0$ and $x_{bulk,C_2}H_6 = 1$ are the critical pressures of a bulk methane and ethane, respectively. Critical properties of the mixture at the specified composition can be estimated from this plot.

As explained earlier, a phase diagram of the confined mixture in a slit graphite pore with 5.0 nm of separation can be generated as illustrated in **Figure 11b**. A series of phase envelopes of the confined mixture is obtained from the GCMC simulations using the described procedures. The phase envelopes are generated from $T = 200$ K to $T = 270$ K, which is in between the critical temperatures of the confined methane (175 K) and ethane (292 K). Again, the intersection between the critical locus curve and the y-axis at $x_{confined,C_2}H_6 = 0$ and $x_{confined,C_2}H_6 = 1$ are the critical pressures of confined methane and ethane, respectively.

Table 3—Critical properties of confined ethane in different pore sizes.

Separation (H), nm	Critical temperature (T_c)	Critical pressure (p_c)
2.0	215 K or −72.7°F	32 kPa or 5 psi
3.0	258 K or −4.7°F	580 kPa or 84 psi
4.0	281.5 K or 47.0°F	1675 kPa or 243 psi
5.0	292 K or 66.9°F	2450 kPa or 355 psi
6.0	298 K or 76.7°F	3050 kPa or 442 psi
7.0	300 K or 80.3°F	3400 kPa or 493 psi
8.0	302 K or 83.9°F	3650 kPa or 529 psi
9.0	304 K or 87.5°F	3800 kPa or 551 psi
10.0	305 K or 89.3°F	3900 kPa or 566 psi
Bulk Fluid	305.3 K or 89.9°F	4884 kPa or 708 psi

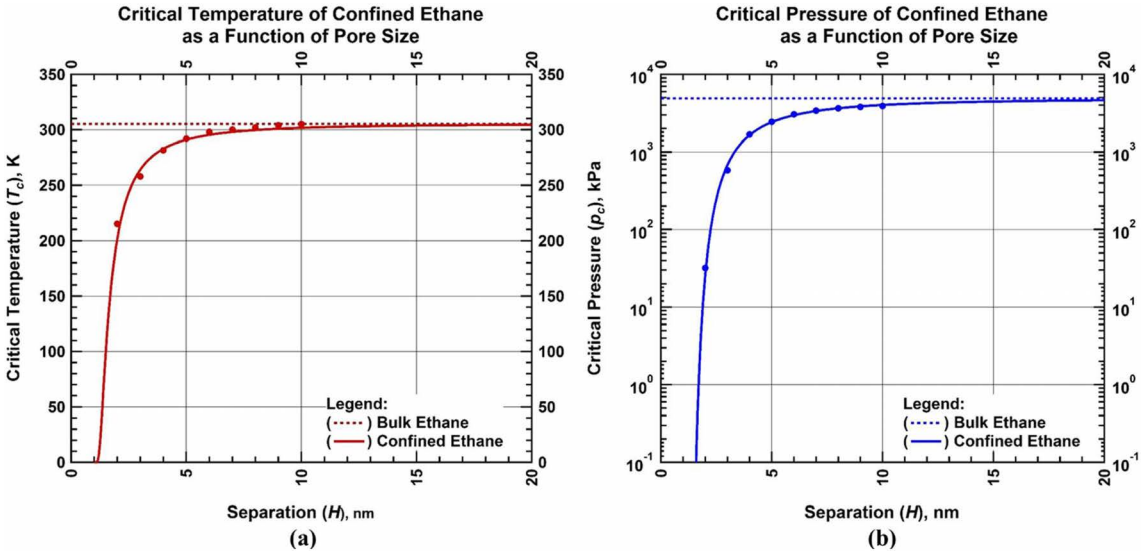

Figure 10—(a) Plot of critical temperature and (b) critical pressure of confined ethane versus separation of a slit graphite pore (representing kerogen in shale reservoir).

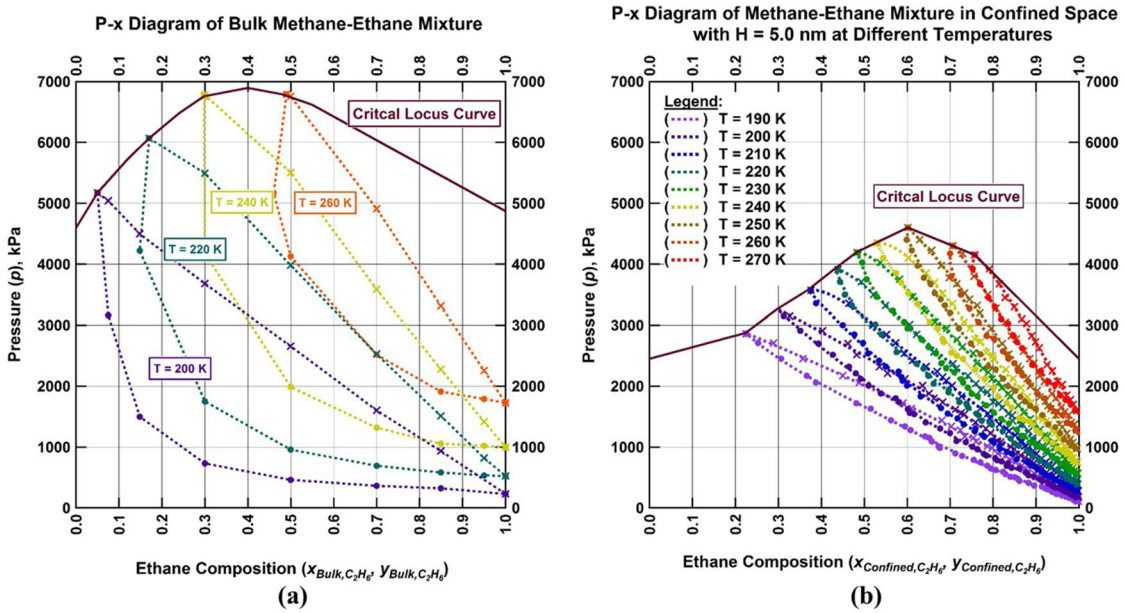

Figure 11—Comparison of bulk methane-ethane mixture phase diagram (a) and that of the confined mixture (b).

Table 4—Eagle Ford reservoir temperature and pressure.

Temperature (T)	Pressure (p)
237°F - 352°F or 387 K - 451 K	6300 psi - 11400 psi 43 MPa - 79 MPa

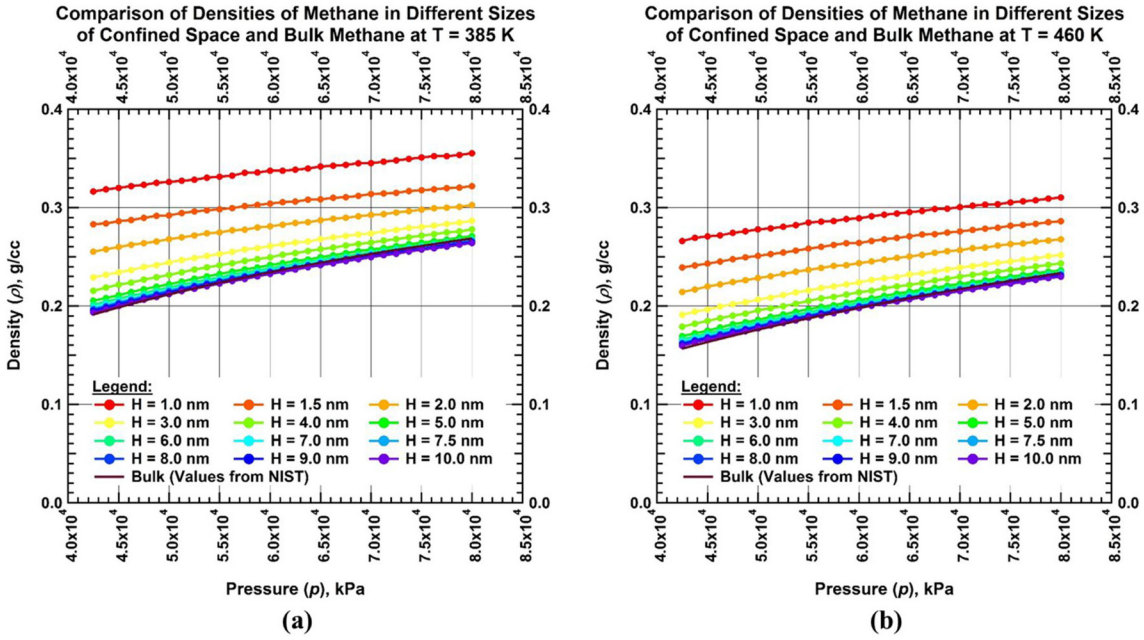

Figure 12—Comparison of bulk and confined methane densities at the (a) minimum and (b) maximum Eagle Ford shale reservoir temperatures

It can be observed that at the same temperature, the shapes and magnitudes of the bulk and confined phase envelopes change dramatically because of the restricted environment existent in kerogen pores of shale reservoirs. Furthermore, the subsequent shift of the critical locus curve of the mixture is in the direction of lower critical temperature and pressure, as similarly observed with the pure components.

Deviation of Confined Fluid Density from the Bulk Density at Reservoir Conditions

In the above sections, the phase diagrams and critical properties of pure components of methane and ethane and their mixtures in nano-scale different from those in actual reservoir conditions. As a result, new GCMC simulations were carried out to obtain fluid densities of pure components of methane and ethane at reservoir conditions. **Table 4** summarizes the ranges of Eagle Ford reservoir temperatures and pressures obtained from Orangi et al. (2011). In this work, according to the reservoir properties listed in Table 4, the possible lower and upper limits of the temperatures used in the molecular simulations are $T = 385$ K and $T = 460$ K, respectively, and the pressure is varied from 42.5 MPa to 80 MPa for both cases.

The isotherms obtained from the GCMC simulation are converted to the confined fluid densities using Equation (5) and compared with the bulk densities from the NIST Chemical WebBook database. The absolute maximum deviation for the confined fluid densities compared with the bulk properties can be calculated using the following formula:

$$\%\, Max.\, Dev. = \frac{|\rho_{confined} - \rho_{bulk}|}{\rho_{bulk}} \times 100\% \tag{6}$$

Methane **Figures 12a** and **12b** illustrate densities of the confined methane in different sizes of slit graphite pores at $T = 385$ K and $T = 460$ K, respectively. In both cases, it can be observed that the confined density is higher than the bulk density at the same condition. In particular, the fluid density in

Table 5—Absolute maximum deviation of confined methane densities from bulk methane

Separation (H), nm	% of Absolute maximum deviation from bulk methane at T = 385 K	at T = 460 K
1.0	65.3 %	69.8 %
1.5	47.9 %	52.6 %
2.0	33.4 %	36.7 %
3.0	19.6 %	22.0 %
4.0	12.5 %	14.1 %
5.0	7.3 %	8.1 %
6.0	5.3 %	6.1 %
7.0	3.7 %	4.7 %
7.5	3.0 %	3.9 %
8.0	2.6 %	3.5 %
9.0	1.7 %	2.6 %
10.0	1.7 %	2.0 %

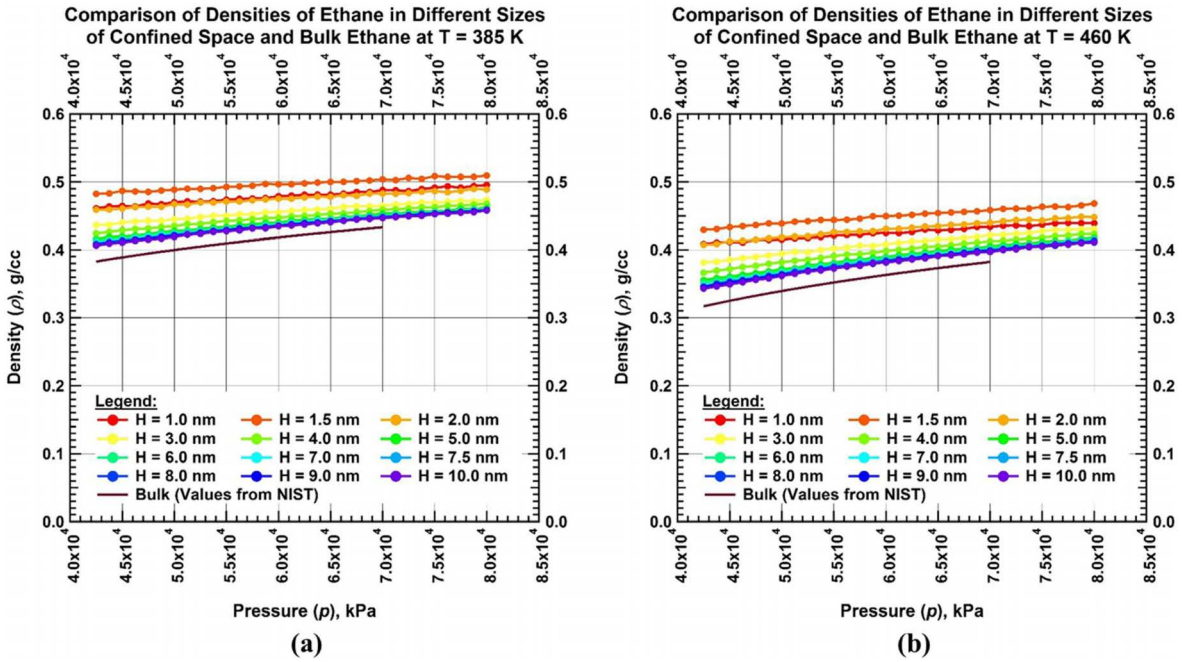

Figure 13—Comparison of bulk and confined ethane densities at the (a) minimum and (b) maximum Eagle Ford shale reservoir temperatures

smaller pores deviates from the bulk density more than that in bigger pores. This is because of the strength of the attractive potential allows more molecules to populate the system and this effect is stronger as the pore size decreases.

The absolute maximum deviations of the confined methane in different pore sizes from the bulk fluid are summarized in **Table 5**. At these reservoir conditions, huge deviations of confined methane densities (~70%) occur when $H = 1.0$ nm due to a strong effect of confinement of kerogen pore in the shale reservoir. However, it becomes less significant when the pore size increases as the deviations reduce to lower than 5% when $H \geq 7.0$ nm.

Ethane **Figures 13a** and **13b** illustrate densities of confined ethane in different sizes of slit graphite pores at $T = 385$ K and $T = 460$ K, respectively. Similar to the previous case, the confined density is higher than the bulk density. In particular, when $H \geq 1.5$ nm, the fluid density in smaller pores deviate from the bulk density more than that in bigger pores. However, it is noticed that the fluid density in the

Table 6—Absolute maximum deviation of confined methane densities from bulk ethane

Separation (H), nm	% of Absolute maximum deviation from bulk methane at T = 385 K	at T = 460 K
1.0	20.4 %	28.9 %
1.5	26.0 %	35.5 %
2.0	19.9 %	28.6 %
3.0	14.0 %	20.4 %
4.0	10.8 %	15.6 %
5.0	8.6 %	12.2 %
6.0	8.0 %	10.9 %
7.0	7.2 %	9.7 %
7.5	7.0 %	9.2 %
8.0	6.7 %	9.2 %
9.0	6.3 %	8.7 %
10.0	6.1 %	8.3 %

slit pore with $H = 1.0$ nm is lower than that in the pore with $H = 1.5$ nm. This is because when $H = 1.0$ nm, the distance between the two layers of the graphite is too short to offer flexibility in terms of molecular orientation and arrangement to the confined ethane. In other words, the separation is less than twice the effective length of the ethane molecule (one adsorbed layer on each side).

The absolute maximum deviations of the confined ethane in different pore sizes from the bulk are summarized in **Table 6**. At the reservoir conditions, huge deviations of confined ethane densities (~36%) occur when $H = 1.5$ nm due to a strong effect of confinement of the kerogen pore in the shale reservoir. However, it becomes less significant when the pore size increases.

According to the deviations of the confined methane and ethane densities from the bulk densities at the reservoir conditions, this may cause intolerable errors in reserves estimation and production forecast calculation if the bulk methane densities are used instead of the proper densities. We note that the pore actually has a distribution of pore sizes, and other restrictions such as pore interconnections may occur which will make the phenomena even more complex. These will be incorporated in future work. However, the present results provide a first approximation of the confinement effect on the phase behavior of fluids in kerogen pores.

Summary of This Work

The confined environment of slit graphite pores representing kerogen pores in shale reservoirs affects fluid molecular behavior. As we observed from the GCMC simulation results, interactions between the surface walls and the fluid molecules will cause changes in the thermodynamic behavior of the hydrocarbon phases (in this study we limited our work to methane and ethane pure components and a methane-ethane mixture). We observed from our simulations that the critical temperature and pressure of pure component methane and ethane are *reduced* as the pore size decreases. In short, the larger the pore size, the less significant is the effect of confinement and their critical properties approach the bulk properties (as expected). For the confined methane-ethane mixtures that we studied, the critical properties and the phase envelope shapes are substantially different from those of the bulk mixture. Moreover, at the reservoir condition, the confined pure component of methane and ethane densities can deviate from their bulk properties by up to 69.8% and 35.5%, respectively. As a result, significant errors could evolve if bulk thermodynamic properties are used in reservoir engineering calculations for shale reservoirs.

Acknowledgement

The authors wish to express appreciation to Dr. Randall Q. Snurr and Dr. Shaji Chempath (Northwestern

University) for permission to use and discussions about the MUSIC software. We also acknowledge and appreciate the Crisman Institute for Petroleum Research in the Harold Vance Department of Petroleum Engineering at Texas A&M University for funding this work. Computer time from the CAT cluster at the Texas A& M Department of Chemical Engineering and time in the TAMU supercomputer facilities are gratefully acknowledged.

Nomenclature

H = Distance or separation between two graphite layers, *Å*
M = Molecular weight, *amu*
n = Number of molecules
N_A = Avogadro's number
p = Pressure, *kPa*
p_c = Critical pressure, *kPa*
r_{ij} = Distance between the two particles, *Å*
T = Temperature, *K*
T_c = Critical temperature, *K*
$V_{Unit\ Cell}$ = Volume of simulated unit cell excluding the volume occupied by the graphite slab, cm^3
x_{bulk,C_2H6} = Ethane molar composition in the bulk system
$x_{confined,C_2H6}$ = Ethane molar composition in liquid phase in the confined system
$y_{confined,C_2H6}$ = Ethane molar composition in vapor phase in the confined system
ϵ_{ii} = Depth of potential trough for the interaction between the two type *i* particles, *kJ/mol*
ϵ_{ij} = Depth of potential trough for the interaction between the type *i* and type *j* particles, *kJ/mol*
ϵ_{jj} = Depth of potential trough for the interaction between the two type *j* particles, *kJ/mol*
μ = Chemical potential, *kJ/mol*
μ_{bulk} = Chemical potential of the bulk system, *kJ/mol*
μ_{bulk,CH_4}^{vapor} = Chemical potential of methane in vapor phase of the bulk system, *kJ/mol*
$\mu_{bulk,C_2H_6}^{vapor}$ = Chemical potential of ethane in vapor phase of the bulk system, *kJ/mol*
$\mu_{confined}$ = Chemical potential of the confined system, *kJ/mol*
$\mu_{confined,CH_4}^{vapor}$ = Chemical potential of methane in vapor phase of the confined system, *kJ/mol*
$\mu_{confined,CH_4}^{liquid}$ = Chemical potential of methane in liquid phase of the confined system, *kJ/mol*
$\mu_{confined,C_2H_6}^{vapor}$ = Chemical potential of ethane in vapor phase of the confined system, *kJ/mol*
$\mu_{confined,C_2H_6}^{liquid}$ = Chemical potential of ethane in liquid phase of the confined system, *kJ/mol*
ρ_{Bulk} = Density of bulk fluid, *g/cc*
$\rho_{Confined}$ = Density of confined fluid, *g/cc*
σ_{ii} = Distance between the two type *i* particles at which the inter-particle potential is zero, *Å*
σ_{ij} = Distance between the type *i* and type *j* particles at which the inter-particle potential is zero, *Å*
σ_{jj} = Distance between the two type *j* particles at which the inter-particle potential is zero, *Å*

References

Ambrose, R.J., Hartman, R.C., and Akkutlu, Y.I.: "Multi-component Sorbed-phase Considerations for Shale Gas-in-place Calculations," paper SPE 141416 presented at the 2011 SPE Production and Operations Symposium, Oklahoma City, OK, USA, 27-29 March.

Ambrose, R.J., Hartman, R.C., Diaz-Campos, M., Akkutlu, Y.I., and Sondergeld, C.H.: "Shale Gas-in-place Calculations Part I: New Pore-Scale Considerations," *J. Pet. Tech*. **17** (1): 219–229. SPE-131772-PA. http://dx.doi.org/10.2118/131772-PA.

Bloomer, O.T., Gami, D.C., and Parent, J.D.: "Physical-Chemical Properties of Methane-Ethane Mixtures," *Research Bulletin, Institute of Gas Technology* **22**.

Curtis, M.E., Ambrose, R.J., Sondergeld, C.H., and Rai, C.S.: "Structural Characterization of Gas Shales on Micro- and Nano-Scales," paper SPE 137693 presented at the 2010 Canadian Unconventional Resources and International Petroleum Conference, Calgary, AB, Canada, 19-21 October.

Darabi, H., Ettehad, A., Javadpour, F., and Sepehrnoori, K.: "Gas Flow in Ultra-tight Shale Strata," *J. Fluid Mech*. **710**: 641–658. http://dx.doi.org/10.1017/jfm.2012.424

Fathi, E., Tinni, A., and Akkutlu, Y.I.: "Shale Gas Correction to Klinkenberg Slip Theory," paper SPE 154977 presented at the Americas Unconventional Resources Conference, Pittsburgh, PA, USA, 5-7 June.

Freeman, C.M.: "A Numerical Study of Microscale Flow Behavior in Tight Gas and Shale Gas Reservoir Systems," paper SPE 141125-STU presented at the 2010 SPE International Student Paper Contest at the SPE Annual Technical Conference and Exhibition, Florence, Italy, 19-22 September.

Hirunsit, P., and Balbuena P.B.: "Effects of Confinement on Water Structure and Dynamics: A Molecular Simulation Study," *J. Phys. Chem.* **111** (4): 1709–1715. http://dx.doi.org/10.1021/jp063718v

Jorgensen, W.L., Madura, J.D., and Swenson, C.J.: "Optimized Intermolecular Potential Functions for Liquid Hydrocarbons," *J. Am. Chem. Soc*. **106** (22): 6638–6646. http://dx.doi.org/10.1021/ja00334a030

Kanda, H., Miyahara, M., and Higashitani, K.: "Triple Point of Lennard-Jones Fluid in Slit Nanopore: Solidification of Critical Condensate," *J. Chem. Phys*. **120** (13): 6173–6179. http://dx.doi.org/10.1063/1.1652431

Kurniawan, Y., Bhatia, S.K., and Rudolph, V.: "Simulation of Binary Mixture Adsorption of Methane and CO_2 at supercritical conditions in carbons," *AIChE J*. **52** (3): 957–967. http://dx.doi.org/10.1002/aic.10687

Moore, E.B., Ezequiel de la Llave, Welke, K., Scherlisb, D.A., and Molinero, V.: "Freezing, Melting and Structure of Ice in a Hydrophilic Nanopore," *Physical Chemistry Chemical Physics* **12** (16): 4124–4134. http://dx.doi.org/10.1039/B919724A

Nagarajan, N.R., Hanapour, M.M., and Arasteh, F.: "Critical Role of Rock and Fluid - Impact on Reservoir Performance on Unconventional Shale Reservoirs," paper SPE 168864 presented at the Unconventional Resources Technology Conference, Denver, CO, USA, 12-14 August.

Orangi, A., Nagarajan, N.R., Hanapour, M.M., and Rosenzweig, J.: "Unconventional Shale Oil and Gas-Condensate Reservoir Production, Impact of Rock, Fluid, and Hydraulic Fractures," paper SPE 140536 presented at the 2011 SPE Hydraulic Fracturing Technology Conference and Exhibition, The Woodlands, TX, USA, 24-26 January.

Shabro, V., Torres-Verdin, C., and Javadpour, F.: "Numerical Simulation of Shale-Gas Production: from Pore-Scale Modeling of Slip-Flow, Knudsen Diffusion, and Langmuir Desorption to Reservoir Modeling of Compressible Fluid," paper SPE 144355 presented at the 2011 SPE North American Unconventional Gas Conference and Exhibition, The Woodlands, TX, USA, 14-16 June.

Vandenbroucke, M.: "Kerogen: from Types to Models of Chemical Structure," *Oil & Gas Science Technology - Rev*. IFP **58** (2): 243–269. http://dx.doi.org/10.2516/ogst:2003016 http://webbook.nist.gov/chemistry/fluid/

Zarragoicoechea, G.J., and Kuz, V.A.: "Critical Shift of a Confined Fluid in a Nanopore," *Fluid Phase Equilibria* **220** (1): 7–9